Title

Spaceborne applications of P band imaging radars for measuring forest biomass

Journal

IEEE Transactions on Geoscience and Remote Sensing, 33(5)

ISSN

0196-2892

Authors

Rignot, EJ
Zimmermann, R
van Zyl, JJ

Publication Date

1995

DOI

10.1109/36.469480

Spaceborne Applications of P Band Imaging Radars for Measuring Forest Biomass

Eric J. Rignot, *Member, IEEE,* Reiner Zimmermann, and Jakob J. van Zyl, *Member, IEEE*

Abstract—**In three sites of boreal and temperate forests, P band HH, HV, and VV polarization data combined estimate total aboveground dry woody biomass within 12 to 27% of the values derived from allometric equations, depending on forest complexity. Biomass estimates derived from HV-polarization data only are 2 to 14% less accurate. When the radar operates at circular polarization, the errors exceed 100% over flooded forests, wet or damaged trees and sparse open tall forests because double-bounce reflections of the radar signals yield radar signatures similar to that of tall and massive forests. Circular polarizations, which minimize the effect of Faraday rotation in spaceborne applications, are therefore of limited use for measuring forest biomass. In the tropical rain forest of Manu, in Peru, where forest biomass ranges from 4 kg m^{-2} in young forest succession up to 50 kg m^{-2} in old, undisturbed floodplain stands, the P band horizontal and vertical polarization data combined separate biomass classes in good agreement with forest inventory estimates. The worldwide need for large scale, updated, biomass estimates, achieved with a uniformly applied method, justifies a more in-depth exploration of multi-polarization long wavelength imaging radar applications for tropical forests inventories.**

I. Introduction

SEVERAL experiments demonstrated that radar backscatter at the longer wavelengths is positively correlated with total above-ground dry woody biomass [1]–[4]. Comparison of radar data acquired at C, L, and P band frequencies showed that the sensitivity and correlation of radar backscatter with woody biomass increases with increasing radar wavelength and is highest at the P band frequency (68 cm wavelength). At that frequency, HH and HV polarization (HV is horizontally received and vertically transmitted) provide a greater sensitivity to woody biomass than VV polarization. Modeling studies showed that P band HV polarized signals are dominated by branch scattering from the larger and lower primary branches of the forest canopy [5]–[8]. As branch scattering is mainly controlled by the size, geometry and dielectric properties of the branches, HV polarized returns are correlated with the fresh branch biomass and forest type. At HH polarization, trunk-ground scattering eventually dominates branch scattering at the high biomass levels. Trunk-ground scattering is mainly controlled by the height, diameter and water content of the tree-trunks, and the wetness, slope and aspect of the ground layers. As a result, HH polarized signals are correlated with the fresh stem biomass—itself a major fraction of total biomass [9]–[11]—and the wetness and surface topography of the ground layers. At VV polarization, trunk-ground interactions are dominated by branch scattering and VV polarized signals are correlated with the fresh branch biomass and forest type, as for HV polarization, and are less sensitive to ground layer conditions. In mono-species, homogeneous forests on nearly level terrain, P band multi polarization backscatter and total biomass are positively correlated up to biomass levels of about 20 kg m^{-2}. With a sensitivity to biomass up to 20 kg m^{-2}, a P band radar could already map the woody biomass of woodland [12]–[14], boreal forests [15] and a significant portion of temperate forests [16]. Beyond 20 kg m^{-2}, radar backscatter values tend to saturate and the retrieval of forest biomass is more complicated than that of a simple linear regression between HV polarization backscatter and woody biomass. Combinations of several polarizations [4] (to include both branch and trunk scattering terms) and/or frequency ratios (to utilize the change in penetration depth of multi frequency signals versus biomass) may help extend the range of sensitivity of the radar data beyond 20 kg m^{-2}. Indepth studies of forests where biomass commonly exceeds 20 kg m^{-2} are however needed to develop an inversion algorithm at these high biomass levels. In conclusion, long wavelength imaging radars have already a unique potential for mapping the aboveground biomass of a large portion of the world's forests, for identifying regions of deforestation and regrowth and for estimating the rates of deforestation and regrowth.

In spaceborne applications, long wavelength imaging radars are affected by Faraday rotation because plane-waves traveling through the ionosphere split into two circularly polarized waves having opposite senses of rotation and different phase velocities. As a result, the plane-wave returns from its journey through the ionosphere with a plane of polarization that has been rotated relative to its original position. The amount of Faraday rotation depends on the electron density profile in the ionosphere, the earth's magnetic field, and increases with the square of the radar frequency [17]. The maximum likely value for Faraday rotation at P band (400 MHz) is 675° during the day and 67° at night. At L band (1.25 GHz), the predicted maximum effect is 69° rotation during the day and 7° at night. The resulting phase and amplitude errors not only affect the estimation of forest biomass from the radar data but the basic processing of the SAR data as well.

In April and October of 1994, the SIR-C/X-SAR radar onboard the space shuttle Endeavour gathered the first polarimetric, spaceborne, radar images of the earth at both C and L band. During the two periods of observation, the JPL calibration team reported cross-talk values between H and V

Manuscript received December 9, 1994; revised May 2, 1995. This work was performed at the Jet Propulsion Laboratory, California Institute of Technology, under contract with the National Aeronautics and Space Administration.

The authors are with the Jet Propulsion Laboratory, California Institute of Technology, Pasadena CA 91109 USA.

IEEE Log Number 9513900.

polarization consistently below 30 dB at L band, day and night [18]. As one would expect a significant amount of cross-talk or leakage between the H polarized and the V polarized channels in the presence of Faraday rotation, these results suggests that Faraday rotation is negligible at L band at 200 km altitude, even during the day. The situation would be different for a radar orbiting at 800 km altitude as the ionospheric electron density at sunspot maximum peaks at about 400 km altitude [17]. One technique, currently used by Global Positioning System satellites, is to transmit at two frequencies slightly offset from each other (1.575 GHz and 1.228 GHz) and combine the measurements to estimate ionospheric propagation. Since night-time P band Faraday rotation is predicted to be comparable to daytime L band Faraday rotation, similar correction techniques could be developed for operating a spaceborne P band radar at linear polarization at night.

Another possibility is to operate the radar at circular-polarization which is less sensitive to Faraday rotation. To test that approach, we compared biomass values predicted from the radar data at both linear and circular polarizations with biomass values derived from allometric equations. We studied four sites representative of boreal, temperate and tropical forests. The two temperate forest sites were discussed previously in [1] and [2] but no direct comparison between radar-predicted and actual biomass values were made, and circular-polarized data were not considered. The boreal forest site was discussed in [4] but without circular-polarization. The tropical rain forest site is a new study site representative of pristine tropical forests in the Amazon basin. Tropical rain forests play an important role in the short term global carbon cycle [19] because they constitute a large pool of stored carbon. They also remain a challenge to remote sensing studies because of both the high variation in biomass [13] (>20 kg m^{-2}) under often uniform, closed canopies with high leaf area indices [20], and the lack of ground truth information due to their aerial extent and often difficult accessibility.

II. Study Sites and Biomass Estimates

The four example forests cover a wide range of forested areas: 1) maritime pine plantations of the Landes forest, south of Bordeaux, in southwestern France (44.6° North, 1.0° West) [1]; 2) lolloby pine plantations of the Duke University Forest, west of Durham, in North Carolina (36.0° North, 79.0° West) [2]; 3) coniferous and deciduous boreal forests of the Bonanza Creek experimental forest, west of Fairbanks, in Alaska (64.4° North, −148.2° West) [4]; and 4) primary tropical rain forests of the Manu National Park, department of Madre de Dios, in southeast Peru (12.0° South, 70.8° West) [21]–[24].

The Landes forest is the largest plantation forest in France, selected as a prototype of a managed forest ecosystem. The forest contains even-aged maritime pine, *Pinus pinaster* (Ait.) (Pinac.) regularly planted in rows [1]. Total above ground woody biomass measured in 30 stands ranges from 1 kg m^{-2} for the youngest stands up to 15 kg m^{-2} for 46 year old forests. Note that bole biomass (max. 10 kg m^{-2}) was erroneously confused with total biomass in [3].

The Duke University forest contains even aged stands of irregularly spaced lolloby pines, *Pinus taeda* (L.) (Pinac.) regrowing on abandoned agricultural fields, as well as mixtures of deciduous and pine trees. Over 100 forest stands were inventoried, with above ground biomass ranging from 0.1 kg m^{-2} for young regrowth up to 49 kg m^{-2} for 100 year old forests [2]–[3]. As many of these stands were too small in width or in number of pixel elements in the AIRSAR images to yield reliable statistics, we limited the present analysis to the 39 largest stands with biomass ranging from 0.1 to 32 kg m^{-2}. Both the Landes forest and the Duke forest lay on nearly flat terrain, and the forest biomass estimates derived from allometric equations are not known with better than 10% accuracy [3].

The Bonanza Creek experimental forest (BCEF) near Fairbanks, Alaska, is a Long Term Ecological Research site representing the boreal forests of interior Alaska. This natural, undisturbed forest includes several deciduous and evergreen tree species in both floodplain and upland forests. Upland forest types on well-drained, nutrient-rich, and south-facing slopes with no permafrost present include stands of highly productive aspen *Populus tremuloides* (Michx.) (Salicac.), paper birch *Betula papyrifera* (Marsh) (Betulac.) and white spruce *Picea glauca* ([Moench] Voss) (Pinac.). On north facing slopes and poorly drained areas, black spruce *Picea mariana* (Mill.) (Pinac.) forests dominate on permafrost soils. Floodplain forests contain productive stands of balsam poplar *Populus balsamifera* (L.) (Salicac.) and white spruce forming on river alluvium and permafrost-free soils. Young successional stages are dominated by alder *Alnus crispa* ([Ait.] Pursh) (Betulac.) and willow shrubs *Salix spp.* (salicac.). Older, poorly drained terraces underlain by permafrost contain sphagnum bogs and tamarack *Larix laricinoides* (Pinac.) mixed with slow growing black spruce. Total above ground biomass ranges from 0.4 to 22 kg m^{-2} in 21 forest stands [4], with a large, natural, spatial variability in biomass within each stand (up to 34% of the mean stand biomass). The accuracy of the *in-situ* biomass estimates probably is not better than 20%.

The Manu National Park, Peru, located at the remote western edge of the Amazon basin, contains pristine, tropical rain forest types with a striking tree species diversity. The generally humid climate is interrupted by a dry season in July-August. Floodplain succession, various stages of disturbed (mosaic) forests and tall climax forests occur on nutrient rich alluvial soils along the Rio Manu, and mature climax forests on more dry and leached soils on the adjacent hills (Fig. 1). A ground team characterized the major forest types and approximate spatial distribution of vegetation along the accessible areas of the lower Manu river in September 1993. Seventeen 10 m radius plots with representative vegetation types were measured for average tree and canopy height, canopy closure, tree density and understory composition. For two forest types, mosaic forest (20 000 m^2) and mature floodplain forest (22 500 m^2), an extensive biomas inventory was available for analysis from Terborgh [32]. The above ground biomass for all forest types was estimated by applying allometric equations [9] for tropical forests [25]. For *Cecropia membranacea* (Morac.) stands, several estimates of forest volume were available from previous studies in the lower Madre de Dios area [24] and Panama [26] and their results are consistent with our estimations. Reported forest volumes were converted to woody

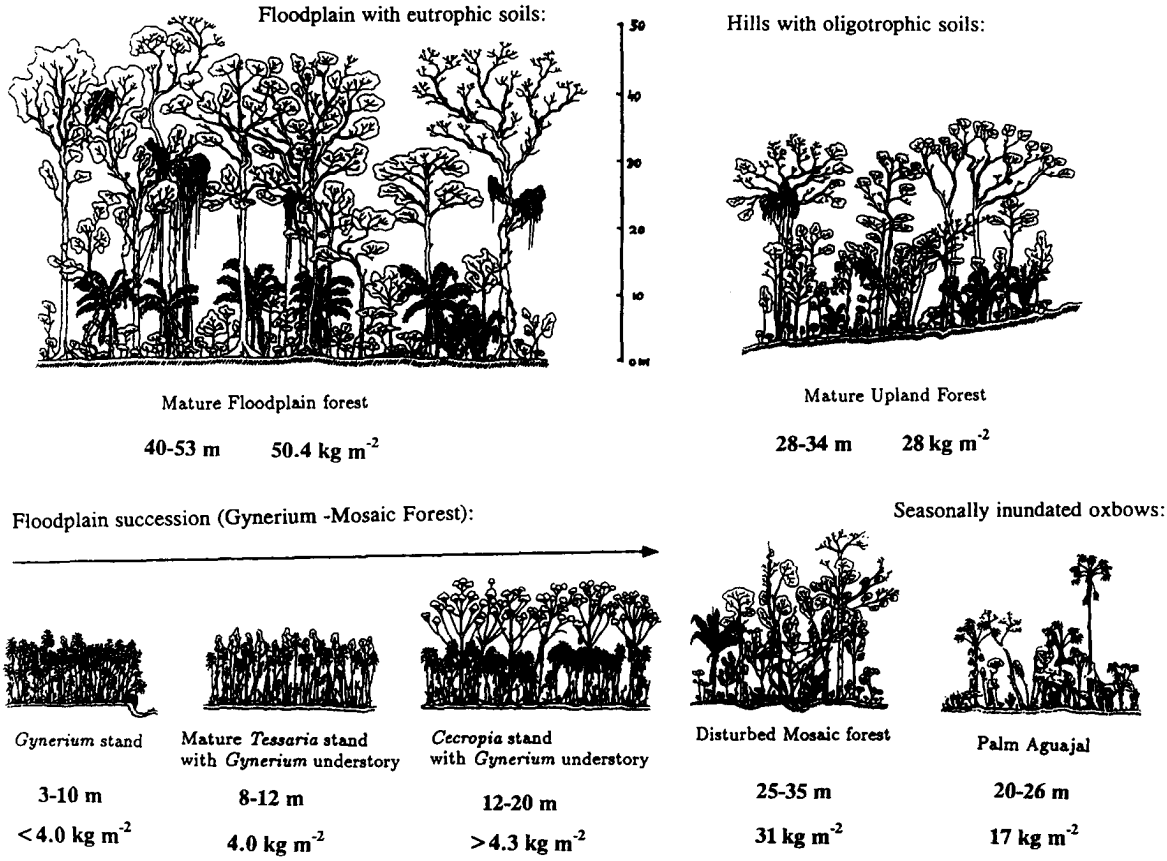

Fig. 1. Major vegetation types of the Rio Manu Area. Forest succession on alluvial floodplains is initiated by disturbance due to flooding during the rain season (October to March). Rapidly growing stands of *Gynerium* and *Tessaria* are eventually replaced by *Cecropia*. Abandoned high river beds may turn into palm dominated areas (Aguajales) with seasonally varying degree of standing water. In undisturbed areas, a mosaic forest develops which will eventually become a mature floodplain forest after 100–200 years. On adjacent hills, the forest is undisturbed, but lower nutrient availability and temporal soil drought cause the development of a shorter forest canopy with seasonal deciduousness. (Drawings: R. Zimmermann)

biomass by using a wood density of 0.5 to account for the light wood of this species compared to the reported average value of 0.62 or 0.69 for tropical woods [11]. Above-ground dry biomass of early forest succession with *Tessaria integrifolia* (Asterac.) and *Gynerium sagittatum* (Poac.) 10 m in height was estimated to be 4 kg m^{-2}. In *Gynerium-Cecropia* forest, 17 m in height, woody biomass is 4.3 kg m^{-2}. On abandoned high river channels with an annually varying water table, palm swamps (Aguajales) may develop. The dominating species in the open canopy is the palm *Mauritia flexuosa syn. reflexa* (Palmae) which reaches 25–30 m height. The understory varies from open sand spots with xerophytic shrubs to permanently flooded areas with dense understory (3–5 m) of banana-like *Heliconia episcopalis* (Musac.) species. Aboveground biomass in a permanently inundated Aguajal (max. 22 m height) was estimated to be 13 kg m^{-2}, 17 kg m^{-2} in a dry and open Aguajal (26 m), and 18 kg m^{-2} in a typical Aguajal (28 m) with moist soil and a high palm density. Broadleaf forest types along the Rio Manu are evergreen to semideciduous with wide variations in canopy structure. In the floodplain, we calculated for a mosaic forest (>27 m) on rich alluvial soil a biomass of 31 kg m^{-2}. Subplot biomass ranged from open areas with 10.1 kg m^{-2} to 81.2 kg m^{-2} (s.d. = 17.9 kg m^{-2}; n = 32 parcels of 625 m^2) [32]. On adjacent hills, forests vary from tall stands with closed canopies to open semideciduous stands. We calculated 28 kg m^{-2} for a semideciduous upland forest (30 m) and 46 kg m^{-2} for a tall forest (40 m) with closed overstory. For these two stands the estimated leaf area index (6.4) was very similar, and the apparent large difference of below-canopy biomass probably results from differences in water and nutrient availability for tree growth. Total above ground biomass of a tall (>50 m), old grown floodplain forest at Cocha Cashu, Rio Manu, was estimated to be 50.4 kg m^{-2}. Individual subplots ranged from gaps with 13.7 kg m^{-2} to dense areas with 114.2 kg m^{-2} (s.d. = 29.6 kg m^{-2}; $n = 25$ parcels of 900 m^2) [32]. This value probably represents the highest above-ground biomass accumulation found in this area due to the large size of individual trees reaching emergent tree heights of 53 m, with diameter at breast height (dbh) of 3 m, and a closed canopy of dominant trees with dbh between 0.9 and 2.4 m [27]. Higher forest volumes are however possible and have been repeatedly reported for temperate coastal rain forests at higher latitudes [28]. Because the impressive, mature floodplain forests cover relatively small areas, the average above-ground biomass weighted by the area covered by each species must be lower. For comparison, reported average maximal biomass values for forested areas without human impact in tropical Asia are 45–54 kg m^{-2} for moist lowland, 35–45 kg m^{-2} for lowland seasonal and 24 kg m^{-2} for dry seasonal types [29]. An exceptional high value was found for

TABLE I
AVERAGE DIFFERENCE BETWEEN RADAR-PREDICTED BIOMASS AND ACTUAL BIOMASS EXPRESSED IN PERCENTAGE OF ACTUAL BIOMASS FOR DIFFERENT COMBINATIONS OF RADAR CHANNELS IN THREE DIFFERENT FOREST SITES. R^2 IS THE R-SQUARED COEFFICIENT OF THE REGRESSION

Forest Site (Date Acq.)	Polarization Combination	Error Linear Pol. % (r^2)	Error Circular Pol. % (r^2)	Polarization Combination
Landes, Fr (08-16-89)	HH, HV, VV	12 (0.99)	11 (0.99)	RL, RR
	HV	14 (0.99)	12 (0.99)	RR
Duke, NC (09-02-89)	HH, HV, VV	27 (0.94)	34 (0.90)	RL, RR
	HV	32 (0.91)	45 (0.82)	RR
BCEF, AK (07-21-93)	HH, HV, VV	18 (0.99)	27 (0.97)	RL, RR
	HV	31 (0.91)	38 (0.94)	RR
BCEF, AK (05-03-91)	HH, HV, VV	30 (0.95)	107 (0.87)	RL, RR
	HV	45 (0.85)	131 (0.78)	RR

the mature building phase of a lower montane rain forest in New Guinea, with 77.3 kg m^{-2} and a range from 62.6 kg m^{-2} to 92.5 kg m^{-2} [33].

III. PREDICTED VERSUS ACTUAL BIOMASS OF BOREAL AND TEMPERATE FORESTS

For each test site, we extracted the radar response of the forest from polygonal areas where forest inventories had been conducted [1]–[4]. A multiple linear regression fit was then performed independently for each site to derive an expression relating the natural logarithm of the stand biomass, $Log(B)$, to the multi-polarization P band radar backscatter values. Each regression is of the form

$$Log(B) = a0 + a1\sigma^o_{HV} + a2(\sigma^o_{HV})^2 + b1\sigma^o_{HH} + b2(\sigma^o_{HH})^2 + c1(\sigma^o_{HH} - \sigma^o_{VV}) + c2(\sigma^o_{HH} - \sigma^o_{VV})^2 \quad (1)$$

where a_i, b_i, c_i are the regression coefficients and σ^o_{HV} denotes the radar backscatter value at HV polarization expressed in dB. When only HV polarization is used, we have $b_i = 0$ and $c_i = 0$. Similar regressions were derived to relate biomass to a polynomial in σ^o_{RR} and σ^o_{RL} (right circular received and left circular transmitted). The regression coefficients for the case where all three linear polarizations are used are listed in Table II. Predicted biomass levels from the radar data were then compared to actual biomass levels. An error was computed as the average absolute difference between predicted and actual biomass, expressed in percent of actual biomass. This error measures the degree of spread between the points used in the regression analysis and the points obtained from a best fit of the data (Table I). We find this measure more representative of the degree of confidence that can be placed in the radar estimates of biomass than, for instance, the coefficient of determination, r^2, which is usually greater than 90% (Table I); or the root mean square error since the error in predicted biomass increases almost linearly with biomass.

For the Landes forest, the average error in predicted biomass at both linear and circular polarization is 12%, and 14% at HV polarization. These errors are very low and comparable to the precision of the surface estimates.

For the Duke University forest, the error rate of P band polarimetry data is 27%, and 32% at a single polarization. This accuracy is lower than for the Landes forest but the stands are less homogeneous, not dominated by a single tree specie, and of much higher biomass (17 kg m^{-2} on average for Duke versus 8 kg m^{-2} for Landes). Linear and circular polarizations yield similar results, except for two stands of relatively low biomass where circular-polarized signals overestimate the woody biomass. In these stands, the HH-VV phase difference is 31° greater than that recorded in neighboring stands of similar biomass and σ^o_{RR} is several dB larger.

For BCEF, the error rate is 18% with the July 1993 P band polarimetry data. The same regression curve was applied for all tree species in the BCEF scene. The predicted biomass levels are 14% less accurate at HV polarization. The largest errors are recorded for alder stands and two mixed stands of white spruce and balsam poplar trees. Alder stands were completely damaged in 1992, most likely a result of river flooding. HH polarized backscatter was unusually large probably because of the abundance of tree trunks laying on the ground, and HV polarized backscatter was large probably because of enhanced depolarization of the radar signals through multiple scattering interactions within the slanted, broken trunks of alder trees. Even at linear polarization, the biomass of alder stands is overestimated by 100%. The biomass of these stands was correctly estimated using the radar data collected in May 1991, prior to the destruction of the stands [4]. Analysis of other frequencies would be needed to identify this part of the forest as severely damaged in 1993. Similarly, in two mixed stands of white spruce and balsam poplar trees, forest biomass was overestimated by >100% at circular polarization. The HH-VV phase difference of these two stands was 90° on average and 40° larger than that observed in other forest stands of similar biomass. We visited one of these stands in 1991 and found that balsam poplar trees were rotten, with very wet tree trunks. Strong double-bounce interactions between the soaked tree trunks and the ground layers may explain the large polarimetric phase differences recorded in those stands, and the resulting overestimates of woody biomass at circular polarization. The same trend was observed in the data collected on May 3, 1991, during a period of intense river flooding. Error rates exceeded 100% at circular polarization and 30% at linear polarization on May 3. Between flooded and dry conditions, the HH-VV phase difference of mature white spruce and balsam poplar floodplain stands decreased from 100° (May 3, 91) to 54° (July 21, 93). As we shall show next, large polarimetric phase differences increase the RR polarized radar backscatter values and result in an overestimation of the biomass.

Forests can be reasonably assumed to be azimuthally symmetric distributed targets, in which case the components of the scattering matrix S_{HH} and S_{HV}, as well as S_{VV} and S_{HV}, are uncorrelated, and $S_{HV} = S_{VH}$ [30]. The average cross products at circular polarization are then computed from the scattering matrix elements as

$$< S_{RL}S^*_{RL} >= \frac{< S_{HH}S^*_{HH} >}{4} + \frac{< S_{VV}S^*_{VV} >}{4} + 0.5Re(< S_{HH}S^*_{VV} >) \quad (2)$$

$$< S_{RR}S^*_{RR} >= \frac{< S_{HH}S^*_{HH} >}{4} + \frac{< S_{VV}S^*_{VV} >}{4} + < S_{HV}S^*_{HV} > -0.5Re(< S_{HH}S^*_{VV} >). \quad (3)$$

TABLE II
REGRESSION COEFFICIENTS FOR: $Log(B) = a0 + a1\sigma^o_{HV} + a2(\sigma^o_{HV})^2 + b1\sigma^o_{HH} + b2(\sigma^o_{HH})^2 + c1(\sigma^o_{HH} - \sigma^o_{VV}) + c2(\sigma^o_{HH} - \sigma^o_{VV})^2$, WHERE B IS THE TOTAL WOODY BIOMASS IN TONS/HA OR 10^1 KG M^{-2}

Forest Site	a0	a1	a2	b1	b2	c1	c2
Landes, Fr (CM1115)	7.5336	0.2518	0.0027	-0.1843	-0.0155	-0.2146	0.0485
Duke, NC (CM4042)	2.9789	-0.9672	-0.0498	0.8350	0.0665	0.4555	-0.0576
BCEF, AK (CM3762)	12.8115	0.9746	0.0189	-1.0541	-0.0766	-0.3304	0.0324
Manu, Peru (CM3700)	23.5723	2.2734	0.0551	-1.4280	-0.1029	-0.5029	0.0333

When the HH-VV phase difference is 180° (double-bounce reflections) and S_{HH} and S_{VV} are equal in magnitude and highly correlated, (2) and (3) yield $\sigma^o_{RL} \approx 0$ and $\sigma^o_{RR} \approx \sigma^o_{HH} + \sigma^o_{HV}$. Even with S_{HH} and S_{VV} not necessarily highly correlated, (2) and (3) show that σ^o_{RL} will be small and σ^o_{RR} will be large when the HH-VV phase difference is close to 180°. In all our study sites, large values of σ^o_{RR} resulted in an overestimation of forest biomass. This was the case of flooded forests, wet or damaged trees, and sparse and tall forests, where trunk ground scattering is a strong contributor to total radar backscatter. Since these conditions may be encountered in many different types of forests, they severely limit the use of circular polarization for estimating woody biomass.

IV. BIOMASS MAPPING IN TROPICAL RAIN FORESTS

Fig. 2(a) shows a false color composite image of the lower Rio Manu and Rio Pinquina in Peru acquired at P band on June 7, 1993 by the NASA/JPL AIRSAR instrument. In this color representation, red corresponds to double-bounce scattering, green to diffuse scattering and blue to single-bounce scattering. The intensity of each color is proportional to the contribution of each one of the above-mentioned simple form of scattering to total radar backscatter. This image was obtained from a Cloude decomposition of the polarimetric signature of the imaged surface using the algorithm described in [31]. This mathematical decomposition of the scattering matrix provides a quantitative description of the type of interaction of the radar signals with the forest canopy which facilitates data analysis. Major vegetation types are delineated in this scattering mechanism map. Palm forests with an open canopy appear red at the center left of the scene, indicating a scattering dominance from double-bounce interactions. Tall floodplain forests (center and upper part) appear yellow, a combination of double-bounce scattering and volume scattering. Surrounding them, large and dense mosaic forest canopies appear green with red dots, indicating scattering dominance from the branches and occasionally double-bounce reflections. Adjacent to the river, early successional stages of short *Tessaria* forests appear green-brown, thereby dominated by branch volume scattering but with weak radar echoes, consistent with their low branch biomass. Taller *Gynerium* forests in dark green and a zone of *Cecropia* forest in lighter green grow further away from the river. In the top portion of the scene, the upland and hill forests between the Rio Manu and the Andes appear to have a higher component of tall deciduous trees (colored green-yellow) than the floodplain forests (colored green) between the lower Rio Manu and the hill area at the bottom of the scene. We attribute this difference mostly to incidence angle effects and not to a real difference in forest composition. In the hill area to the bottom of the scene, regular hills of 30–50 m elevation yield a pronounced textural modulation of the SAR signal.

In contrast, the L and C band Cloude decompositions (Fig. 1(b) and 1(c)) show much less separability in scattering behavior between major vegetation types. This result may be attributed to the larger penetration of P band signals that interact with subcanopy structures. The higher frequency signals are limited to upper canopy interactions, where distinctions between major vegetation types are less apparent. The blue tone of the C band decomposition illustrates that C band radar returns contain a mixture of volume scattering from the upper branches and single-bounce reflections from the top of the canopy. As the frequency is reduced, the color tone of the forest becomes more yellow, suggesting increasing contributions from trunk ground scattering. This example decomposition is illustrative of the differential penetrability of multifrequency signals into a thick forest canopy, and suggests that HH polarization is the most useful channel for distinguishing vegetation communities of high biomass level.

At circular polarization, P band data did not estimate forest biomass correctly because large HH-VV phase differences in palm forests yield large values of σ^0_{RR} and >100% overpredicted woody biomass. This example shows that polarimetric phase differences are not well correlated with forest biomass. Better radar predictions were obtained using the P band HH, HV, and VV polarization combined with no phase information (Fig. 2(d)). In the biomass map shown in Fig. 2(d), areas where the predicted forest biomass exceeds 30 kg m^{-2} (dark green) are mature floodplain forests where woody biomass is indeed expected to be the largest (Fig. 1). The forest floor in the imaged broadleaf forests was dry at the time of the AIRSAR overflight (the dry season ends in September) so the enhanced radar signature of these stands at HH polarization is not caused by wet ground layers but more likely by tall tree trunks of large diameter. Forest biomass is lower in palm forests (green), which are surrounded by broadleaf forests of higher biomass (dark green). Old meanders, sealed off by freshly deposited sediment and showing as oxbow lakes (Cochas) with open water are mapped as areas of no biomass (black). Low biomass (brown) is estimated along the termini of Cochas, having an early succession of sedges, grasses and shrubs, especially *Annona tessmannii* (Annonac.), which are occasionally intercut by a tall stand of *Heliconia episcopalis* (Musac.) with slightly larger biomass (oxbow at center right of the scene, green). In the expanding meander loop, at the center left of the image, that points down toward the lower border of the river, the early succession of riparian vegetation is well discriminated in the biomass map. Forest succession starts from the beach with short, even-aged stands of fast-growing *Tessaria* shrubs, followed by *Gynerium* stands (6 m

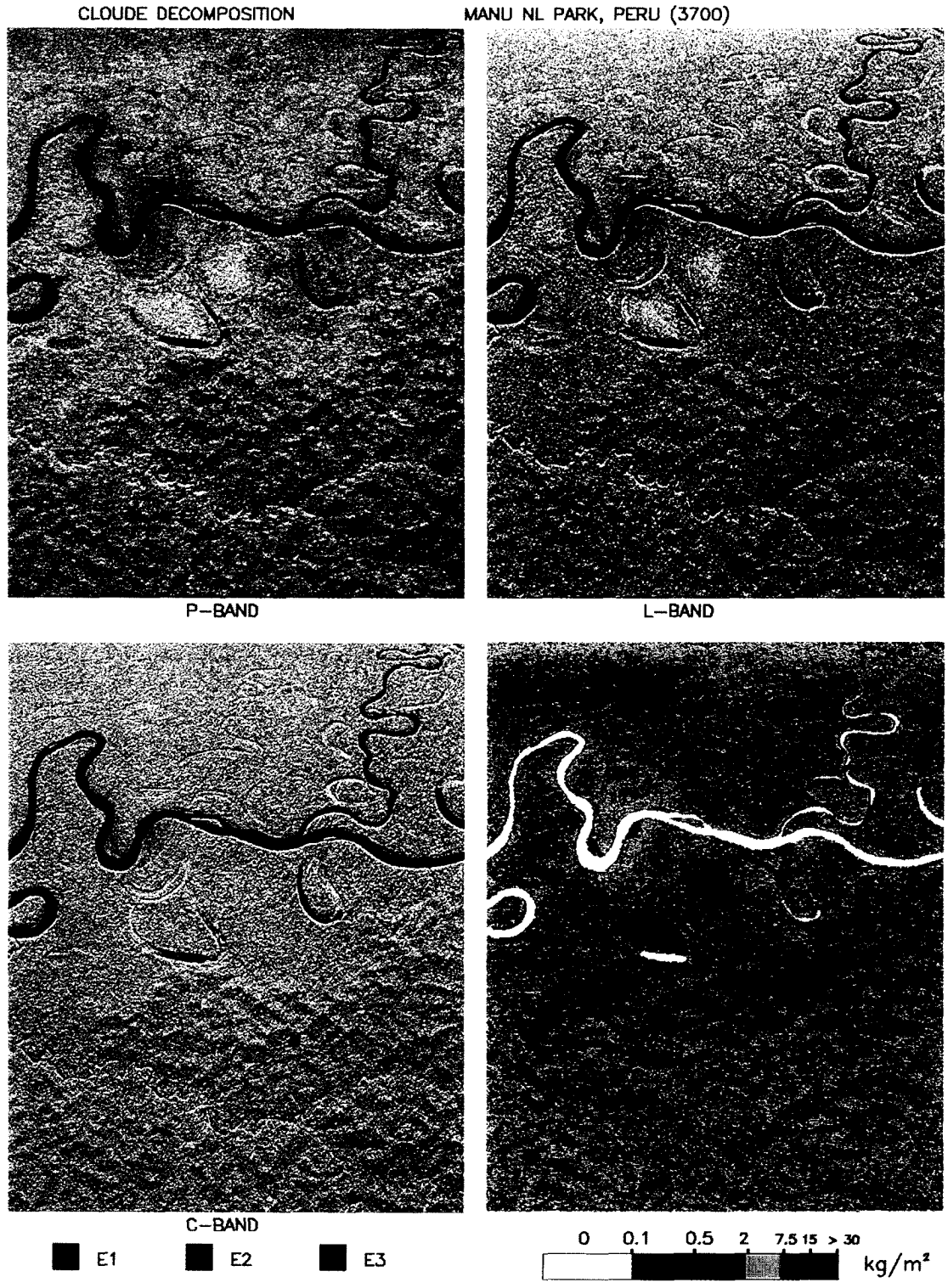

Fig. 2. False color composites of a 10 km x 10 km radar image of the Manu National Park Forest, in southeastern Peru. AIRSAR is flying from left to right, illuminating the surface from the top. (a), (b), and (c) are representations of the Cloude decomposition of polarimetric scattering at (a) P band, (b) L band, and (c) C band. The Rio Manu (flowing from left to right) and Rio Pinquina (entering Rio Manu from the top) appear as dark features. (d) is a map of forest biomass between 0 and >30 kg m^{-2}.

in height) with higher biomass (dark brown). Adjacent are older successional stages of *Tessaria-Gynerium* (10–12 m in height) (light brown), and pure *Gynerium* (yellow). Continuing inland, toward the top of the scene, are higher biomass (blue-green in Fig. 2(d)) deciduous leafless trees species mixed with *Cecropia* (10–26 m) above a 5 m tall understory of *Gynerium*. A mosaic of semideciduous floodplain forest (30–35 m) with higher predicted biomass follows. This type of clearly zoned and highly productive riparian forest succession, where each stage is taller than the previous one, is characteristic of this

area and can be identified at many locations along the river. For instance, to the right of the previous meander, *Gynerium* and scattered *Tessaria* (10–12 m) on the upper bank, and *Gynerium* (5 m) with scattered leafless trees (25 m) on the lower bank were colored light brown and yellow as they indeed correspond to intermediate ranges of low biomass of about 4 kg m^{-2}. The extensive *Cecropia* forests next to these correctly appear as areas of intermediate biomass (yellow).

Within the same type of forest, the P band data correctly distinguished different biomass levels. For instance, the total biomass of the wet palm aguajal was correctly estimated to be 4 to 5 kg m^{-2} lower than that of the dry aguajal and of the typical aguajal. The breaking up of the forest into different biomass units is therefore not only caused by structural differences between forest types but also by actual differences in biomass level. For most of our sites, sample plot areas are however not large enough to permit a direct, quantitative comparison of the radar estimates with the ground estimates. We are currently examining a larger forest inventory dataset collected over 19 plots, each greater than 10 000 m^2 in size [32]. The results of this analysis and an evaluation of the precision of the radar-predicted biomass estimates will be reported in a future paper.

In the hill-areas at the bottom of Fig. 1(d), the spatial variability in radar backscatter is controlled by surface topography. Forest biomass is overestimated in the hills facing the radar looking direction and is underestimated in the slopes facing away from the radar. Over hilly terrain, a digital elevation model of the surface—not available for this study—is needed to correct the data from topography-induced calibration errors.

V. Conclusion

A comparison of radar-predicted estimates of forest biomass with forest inventory estimates in three sites of temperate and boreal forests shows that the average absolute error in predicted biomass is 12 to 27% of the actual biomass, depending on forest complexity. These accuracies are only a few percent higher than that obtained from allometric equations, which suggest that the errors introduced in the radar estimation process are small. Linear polarizations yield more reliable estimates than circular polarizations, and the use of three linear polarizations (without phase information) helps significantly to improve the accuracy of the estimates derived from linear cross-polarized data. This result is consistent with the fact that HV signals are correlated with branch biomass, which may or may not be a good indicator of total biomass depending on forest type and biomass level; whereas HH polarization is correlated with stem biomass which is a more direct indicator of total biomass, especially at the high biomass levels.

It is expected that the precision of the radar estimates will increase if structural differences between forest types are accounted for during the inversion of the radar data. Land cover maps are, however, seldomly available and typically require detailed and regular updating to be reliable, which is a very difficult task over large areas. The breaking up of a forest into botanical sub-units may also prove difficult in tropical forests where hundreds of tree species are mixed together. It is therefore important to know how well radar imaging techniques would work in various broad types of forests, even in the absence of very detailed vegetation maps, as was done in this study for boreal, temperate and tropical forests. Further studies are needed to determine whether regression curves developed for broad classes of forest are applicable at the large scale. Preliminary results obtained during the BOREAS experiment showed that the regression equations developed for Alaskan forests (BCEF) in the summer season yield reasonable estimates of forest biomass for the Canadian boreal forests.

Over hilly terrain, correction of the radar data—as well as the *in situ* biomass data—for surface topography effects are needed before data inversion. Studies of this kind are in progress in the Pacific northwest where surface topography—ignored in previous radar studies—is a major factor and woody biomass reaches some of the highest levels in the world ($>>100$ kg m^{-2}). The results combining radar backscatter and topography data acquired by the NASA/JPL SAR instrument and precise forest inventory estimates gathered by researchers at the University of Oregon will be reported in a future paper. In tropical forests, the results obtained in the floodplain forest of Manu are encouraging that long wavelengths imaging radars can assist in estimating their forest biomass and provide results unachievable by any other means, even though biomass levels largely exceed 20 kg m^{-2}. The worldwide need for large scale, updated biomass estimates, achieved with a uniformly applied method, justifies a more indepth exploration of long wavelength imaging radar applications for tropical forests inventories.

Acknowledgment

The authors would like to thank J. Terborgh for providing two extensive ground data sets, R. Oren for a critical review of the manuscript, and S. Billings, B. Chapman, and V. Horna-Rodriguez for help in getting the ground truth data in Peru. They would also like thank T. Le Toan for providing the ground truth data for the Landes forest, E. Kasischke for providing the ground truth data for the Duke University forest, and J. Klein for comments on the manuscript.

References

[1] T. LeToan, A. Beaudoin, J. Riom, and D. Guyon, "Relating forest biomass to SAR data," *IEEE Trans. Geosci. Remote Sensing*, vol. 30, pp. 403–411, 1992.

[2] E. S. Kasischke, L. L. Bourgeau-Chavez, N. L. Christensen, and M. C. Dobson, "The relationship between above-ground biomass and radar backscatter as observed on airborne SAR imagery," in *Proc. 3rd AIRSAR Workshop*, Pasadena, CA, May 23–24, 1991, JPL Pub. 91–30, pp. 11–21, 1991.

[3] M. C. Dobson, F. T. Ulaby, T. LeToan, A. Beaudoin, E. S. Kasischke, and N. Christensen, "Dependence of radar backscatter on conifer forest biomass," *IEEE Trans. Geosci. Remote Sensing*, vol. 30, pp. 412–415, 1992.

[4] E. Rignot, C. Williams, J. B. Way, and L. Viereck, "Radar estimates of aboveground biomass in boreal forests of interior Alaska," *IEEE Trans. Geosci. Remote Sensing*, vol. 32, pp. 1117–1124, 1994.

[5] A. Beaudoin, T. LeToan, S. Goze, E. Nezry, A. Lopes, E. Mougin, C. C. Hsu, H. C. Han, J. A. Kong, and R. T. Shin, "Retrieval of forest biomass from SAR data," *Int. J. Remote Sensing*, vol. 15, pp. 2777–2797, 1994.

[6] C. C. Hsu, H. C. Han, R. T. Shin, J. A. Kong, A. Beaudoin, and T. LeToan, "Radiative transfer theory for polarimetric remote sensing of pine forest," *Int. J. Remote Sensing*, vol. 15, pp. 2943–2954, 1994.

[7] J.J. van Zyl, "The effect of topography on radar scattering from vegetated areas," *IEEE Trans. Geosci. Remote Sensing*, vol. 31, pp. 153–160, 1993.
[8] R. H. Lang, N. S. Chauhan, K. J. Ranson, and O. Kilic, "Modeling P-band SAR returns from a red pine stand," *Remote Sensing Environ.*, vol. 47, pp. 132–141, 1994.
[9] H. Ogawa, K. Yoda, K. Ogina, and T. Kira, "Comparative ecological studies on three main types of forest vegetation in Thailand II. Plant biomass," *Nature and Life in S.E. Asia*, vol. 4, pp. 49–80, 1965.
[10] C. Huttel, "Root distribution and Biomass in three ivory coast rain forest plots," in *Tropical Ecological Systems*, Ecological Studies, E. Medina and F. Golly, Eds. New York: Springer Verlag, 1975, vol. 11, pp. 123–130.
[11] P. M. Fearnside, L. Niwton and F. M. Fernandes, "Rainforest burning and the global carbon budget: biomass, combustion efficiency, and charcoal formation in the Brazilian Amazon," *J. Geophys. Res.*, vol. 98, pp. 16 733–16 743, 1993.
[12] R. H. Whittaker and G. E. Likens, "Carbon in the biota," in *Carbon and the Biosphere*, G. M. Woodwell and E. V. Pecan, Eds., Nat. Tech. Inform. Center, Springfield, VA., pp. 281–300, 1973.
[13] L. E. Rodin, N. I. Bazilevich, and N. N. Rozov, *Productivity of the World Main Ecosystems*, D. E. Reichle, Franklin J. F. Goodall, Eds. Washington, DC: National Academy of Sciences, 1975.
[14] H. Lieth, "Primary productivity in ecosystems: Comparative analysis of global patterns," in *Unifying Concepts in Ecology, Proc. Rep. Plen. Sess. First Intern. Congr. Ecol.*, 1975. pp. 67–88.
[15] D. B. Botkin and L. G. Simpson, "Biomass of the North American boreal forest: A step forward toward accurate global measures," *Biochemistry*, vol. 9, pp. 161–174, 1990.
[16] D. B. Botkin, L. G. Simpson, and R. A. Nisbet, "Biomass and carbon storage of the North American deciduous forest," *Biochemistry*, vol. 20, pp. 1–17, 1993.
[17] J. V. Evans and T. Hagfors, *Radar Astronomy*. New York: McGraw-Hill, 1968.
[18] A. Freeman, J. Cruz, B. Chapman, M. Alves. J. Sun, M. Azeem, and S. Shaffer, "First results from SIR-C calibration," in *Proc. Int. Geosci. Remote Sensing Symp. IGARSS'94*, Pasadena, CA, Aug. 8–12, 1994, vol. II, pp. 1079–1081.
[19] B. Bolin, T. Degens, S. Kempe, and P. Ketner, "The global carbon cycle" in *Scope 13*. Chichester: Wiley, 1979.
[20] H. W. Art and P. L. Marks, "A summary table of biomass and net annual primary production in forest ecosystems of the world," in *Forest Biomass Studies, 15th. Int. Union Forest Res. Organ. Congr.*, 1971, Sec. 25, pp. 3–32.
[21] J. Terborgh, *Five New World Primates: A Study in Comparative Ecology*, Princeton, NJ: Princeton Univ. Press, 1983.
[22] J. Terborgh, "Habitat selection in Amazonian birds," in *Habitat Selection in Birds*, M.L. Cody, Ed. New York: Academic, 1985, pp. 311–318.
[23] R. Kalliola, J. Salo, and Y. Mäkinen, "Regeneracion natural de selvas en la Amazonia Peruana 1: dinamica fluvial y sucesion ribereña," in *Memorias del Museo de historia Natural 'Javier Prado' (Lima)*, vol. 18, pp. 1–102, 1987.
[24] W. G. Sanchez, "Aspectos taxonómicos, fitosociologicos y aplicados del género ceropia en el Valle de Kcosñipata y el Manu," Master's thesis, Universdad Nacional de San Antonio Abad del Cusco, Peru, 1976.
[25] FAO-UNESCO-UNEP, *Tropical Forest Ecosystems*, 1978, ch. 10, pp. 233–248.
[26] H. Walter and S. W. Breckle, *Ecological Systems of the Geobiosphere, Tropical and Subtropical Zonobiomes*, vol. 2. Berlin: Springer-Verlag, 1984.
[27] J. A. Tosi, "Zonas de vida natural en El Peru, Instituto Interamericano de Ciencias Agricolas de la OEA Zona Andina," in *Boletin Tecnico*. 1960, vol. 5, pp. 271.
[28] H. Walter and S. W. Breckle, *Ecological Systems of the Geobiosphere, Temperate and Polar Biomes Other than Northern Eurasia*, vol. 4. Berlin: Springer-Verlag, 1991.
[29] FAO, "Forest resources assessment 1990, tropical countries," FAO Forestry Paper 112, Rome, 1993.
[30] S. V. Nghiem, S. H. Yueh, R. Kwok, and F. K. Li, "Symmetry properties in polarimetric remote sensing," *Radio Sci.*, vol. 27, pp. 693–712, 1992.
[31] J. J. van Zyl, "Application of Cloude's target decomposition theorem to polarimetric imaging radar data," *Proc. SPIE*, vol. 1748 Radar Polarimetry, pp. 184–191, 1992.
[32] J. Terborgh, "Biomass inventories from the Rio Manu area," Peru, unpublished data.
[33] P. J. Edwards and P. J. Grubb, "Studies of mineral cycling in a montane rain forest in New Guinea, I. The distribution of organic matter in the vegetation and soil," *J. Ecol.*, vol. 65, pp. 943–969, 1977.

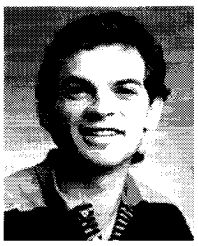

Eric J. Rignot (M'91) was born in Chambon sur Lignon, France, in 1961. He received the Engineer's diploma from the Ecole Centrale des Arts et Manufactures Paris in 1985, the M.S. degrees in aerospace engineering and in electrical engineering in 1987 and 1988 and the Ph.D. degree in electrical engineering in 1991 from the University of Southern California, Los Angeles.

He was employed as a Research Assistant at the University of Southern California in the Department of Aerospace Engineering during 1986–1988. Since then, he has been with the Radar Science and Engineering Section at the Jet Propulsion Laboratory, California Institute of Technology, Pasadena. He is the Principal Investigator for a NASA project utilizing radar data to study the melting facies of the Greenland Ice Sheet, the Principal Investigator of a TOPSAT DCL Project for studying the surface topography and ice motion of the Greenland Ice Sheet using SAR interferometry, a co-investigator on the NASA/BOREAS experiment to utilize SAR-derived forest seasonal state, biomass and type in carbon flux models, a co-investigator on an ERS-1/J ERS-1 forest project to detect changes in environmental state of boreal forests, and a member of the SIR-C Science Team interested in land cover mapping applications, estimation of forest biomass, and interferometry studies of Patagonian outlet glaciers.

Dr. Rignot is a member of AGU.

Reiner Zimmermann received the M.S. degree in botany (1985) and the doctoral degree in plant ecology (1990) from the Department of Plant Ecology, University of Bayreuth, Germany.

From 1986 to 1990 he was the Research Leader of the eco-physiology group in the interdisciplinary acid rain study in the Fichtelgebirge, Northern Bavaria, Germany, where he studied the carbon, nutrient, and water relations of conifers in relation to forest decline phenomena. During that time he was also Visiting Scientist at the Institut National de la Recherche Agronomique I.N.R.A. at Kourou, French Guyana, and at Nancy, France, with studies on water relations and carbon uptake of mediterranean conifers and tropical tree species. In 1990 he joined the Hydrology, Soils, and Ecology Group for Radar Sciences at the Jet Propulsion Laboratory (CALTECH) in Pasadena. His current research activities are comparative studies of water and energy exchange between forests and the atmosphere along latitudinal gradients in evergreen and deciduous forest ecosystems and the relationships between tree dielectric constant, tree water status, canopy structure, and its detection by Synthetic Aperture Radar (SAR). He is currently involved in research projects on mixed deciduous and coniferous forests in Alaska (INF, Fairbanks), Canada (BOREAS), Siberia (Academy of Science Moscow and St. Petersburg), and Germany (University of Bayreuth). He also works on ecophysiological questions at the Duke University, Durham, NC (DOE), where he holds an appointment as Adjunct Professor at the School of the Environment (SOE).

Jakob J. van Zyl (S'85–M'86) was born in Outjo, Namibia, in 1957. He received the Hons. B.Eng. degree *cum laude* in electronics engineering from the University of Stellenbosch, Stellenbosch, South Africa, in 1979, and also received the Siemens prize for best achievement in the graduating class from the electrical engineering department. He received the M.S. and Ph.D. degrees in electrical engineering from the California Institute of Technology, Pasadena, in 1983 and 1986, respectively.

In 1984 he was the recipient of a Schlumberger Foundation fellowship. He was Teaching Assistant for a course on "Physics of Remote Sensing" at the California Institute of Technology from 1983 to 1986. At present he is the Manager of the Radar Science and Engineering Section and the Program Manager for the Airborne Active Microwave Instruments Program at the Jet Propulsion Laboratory, Pasadena, CA. He is a five-year member of the Institute for Electromagnetics Modelling and Applications of The Electromagnetics Academy. His current interests include studying theoretical electromagnetic problems related to polarimetric scattering, remote sensing, and the analysis of polarimetric SAR data.